Letter

Optimal limits of continuously monitored thermometers and their Hamiltonian structure

Mohammad Mehboudi [1,*] Florian Meier [1,†] Marcus Huber [1,2,‡] and Harry J. D. Miller [3,§]

[1] *Vienna Center for Quantum Science and Technology, Atominstitut, Technische Universität Wien, 1020 Vienna, Austria*

[2] *Institute for Quantum Optics and Quantum Information (IQOQI), Austrian Academy of Sciences, Boltzmanngasse 3, 1090 Vienna, Austria*

[3] *Department of Physics and Astronomy, University of Manchester, Oxford Road, Manchester M13 9PL, United Kingdom*

(Received 3 September 2024; accepted 15 January 2025; published 5 February 2025)

We investigate the fundamental and practical precision limits of thermometry in bosonic and fermionic environments by coupling an N-level probe to them and continuously monitoring it. Our findings show that the ultimate precision limit, quantified by the Fisher information, scales linearly with N, offering an exponential improvement over equilibrium thermometry, where the scaling is only $\log^2 N$. For a fixed Hamiltonian structure, we develop a maximum-likelihood estimation strategy that maps the observed continuously monitored trajectories of the probe into temperature estimates with minimal error. By optimizing over all possible Hamiltonian structures, we discover that the optimal configuration is an effective two-level system, with both levels exhibiting degeneracy that increases with N—a stark contrast to equilibrium thermometry, where the ground state remains nondegenerate. Our results have practical implications. First, continuous monitoring is experimentally feasible on several platforms and accounts for the preparation time of the probe, which is often overlooked in other approaches such as prepare and reset. Second, the linear scaling is robust against deviations from the effective two-level structure of the optimal Hamiltonian. Additionally, this robustness extends to cases of initial ignorance about the temperature. Thus, in global estimation problems, the linear scaling remains intact even without adaptive strategies.

DOI: 10.1103/PhysRevA.111.L020401

Introduction. High-precision temperature measurements are crucial for the development of nanoelectronic [1,2] and cold-atom technologies [3,4], with accurate low-temperature sensing now fundamental for experimental tests in condensed matter [5,6], many-body thermalization [7,8], and the realization of small-scale thermodynamic devices [9]. Recent thermometry techniques have been proposed across a wide range of different systems, such as solid-state impurities [10] optomechanical setups [11], quantum gases [12–15], dephased impurities [16], and topological spinless fermions [17]. However, there remains an ongoing search to find methods for probing the temperatures of many-body systems that are simultaneously practical, accurate, and resource efficient [18]. This ultimately entails designing a small probe that can interact with the sample and encode information about its temperature in an optimal manner, with estimation schemes established through either local [18–25] or global methods [26–30].

One common approach is *equilibrium thermometry* [31–36], where temperature estimates are obtained via energy measurements of a thermalized probe. It has been shown that the optimal energy structure of such an equilibrium thermometer is an effective two-level system with a single ground state and a maximally degenerate [$(N-1)$-fold] excited state at an optimal gap $\epsilon^*_{\rm eq}$ [19]. Subsequently, several studies have addressed how to simulate such an energy structure by using physically realizable many-body models [32,35,37–40] and even getting the right scaling and asymptotic behavior with two-body interactions [17,41]. On the other hand, the degenerate energy structure also leads to long equilibration timescales for the probe [42]; if one factors in time as a resource in metrology [43,44], equilibrium thermometry may not be the preferable approach [45]. This instead motivates the use of finite-time probes that encode information about temperature via nonequilibrium dynamics [46–53]. However, in these scenarios the question of optimality is not so clear, particularly due to the need to use adaptive estimation schemes, repeatable state preparations alongside measurements at precise times.

The aim of this Letter is to explore optimal thermometry in an alternative approach based on *continuous monitoring* [54–57]. This is a practical and convenient method that involves monitoring the probe populations across time while out of equilibrium [58]. Since the transition rates governing the dynamics of the probe depend on temperature, one can apply a maximum-likelihood estimation scheme directly to the population trajectories [59]. This clearly has a resource advantage over other approaches that reset or discard the

*Contact author: mohammad.mehboudi@tuwien.ac.at
†Contact author: florian.meier@tuwien.ac.at
‡Contact author: marcus.huber@tuwien.ac.at
§Contact author: harry.miller@manchester.ac.uk

probe after each measurement, and instead makes full use of the information contained in the dynamical history of a *single* probe. With recent advancements in continuous monitoring methods such as photodetection, homodyne/heterodyne detection [60,61], and other quantum nondemolition measurements [62], this approach to thermometry is experimentally realizable.

Given the feasibility of the continuous monitoring approach along with its advantages in terms of resources, one remaining goal is to find the best energy structure for the probe. Using a combination of both analytic and numerical methods, we demonstrate that the optimal structure mirrors that of an equilibrium thermometer, i.e., an effective two-level system with a degenerate ground state and a degenerate excited state. Investigating both fermionic and bosonic samples, we show that the precision of an N-level probe can achieve linear scaling with the number of levels, thereby providing an exponential improvement to equilibrium thermometry methods such as Ref. [19]. Furthermore, this optimal structure and its performance bounds apply universally across all temperature ranges, thus bypassing the need for adaptive measurement scheme such as Ref. [29]. Overall, our results solidify the significant advantages offered by continuously monitored thermometers.

Setup. We will begin by modeling a probe as a finite-dimensional system with N energy levels, which is in weak contact with a thermal sample at inverse temperature $\beta = 1/k_B T$. It is assumed that the population dynamics of the probe follow a Markovian rate equation of typical form

$$\dot{\mathbf{p}}(t) = \mathbf{p}(t)\Gamma, \tag{1}$$

with $\mathbf{p}(t) = [p_1(t), \ldots, p_N(t)]$ being the vector of populations of the energy levels $\{\epsilon_1, \epsilon_2, \ldots, \epsilon_N\}$, and Γ being the transition matrix. The matrix elements Γ_{ij} quantify the rate of jumping from state i into the state j, with conservation of probability ensured by $\Gamma_{ii} = -\sum_{j\neq i}\Gamma_{ij}$. The rates are assumed to satisfy detailed balance, $\Gamma_{ij} = e^{-\beta(\epsilon_j-\epsilon_i)}\Gamma_{ji}$, so that the thermal distribution $\mathbf{p}^{\rm eq} = \{e^{-\beta\epsilon_1}/Z, \ldots, e^{-\beta\epsilon_N}/Z\}$ is stationary, $\mathbf{p}^{\rm eq}\Gamma = 0$, and we further assume this is unique.

In order to use the probe as a thermometer for estimating temperature T, we will follow the scheme introduced in Ref. [58] and continuously monitor its energy over time. This is a jump unravelling process [63], and the schematics of this setup is shown in Fig. 1. The data output of the continuous monitoring over some time window $[0, \tau]$ is represented by a stochastic trajectory of a discrete-time process $\mathbf{X}_\tau = \{(n_0, t_0 = 0), (n_1, t_1), \ldots, (n_m, t_m = \tau)\}$, where each (n_k, t_k) denotes an observation of the n_kth energy level ϵ_{n_k} at an intermediate time $0 \leqslant t_k \leqslant \tau$, where $t_k = k\tau/m$. The probability of this trajectory is of the form $P(\mathbf{X}_\tau) = p(n_0)p(n_1|n_0)\cdots p(n_m|n_{m-1})$ with each transition probability determined by the rates in the master equation (1). Since the trajectory probability is dependent upon the temperature of the sample, $P(\mathbf{X}_\tau) = P(\mathbf{X}_\tau|T)$, we can use the data to construct an estimator $\hat{T}$. For large τ a suitable estimator becomes unbiased and its maximum precision is fixed by the Cramer-Rao bound, which bounds the mean-squared error $\mathrm{Var}\,(\hat{T}) \geqslant 1/F(T)$ in terms of the Fisher information (FI), defined $F(T) := \langle[\partial_T \ln P(\mathbf{X}_\tau|T)]^2\rangle$. As the system obeys an order-1 Markov process with unique fixed point $\mathbf{p}^{\rm eq}$, we can use a result from Ref. [59] to express the Fisher information directly in terms of the master equation rates and thermal populations $p_i^{\rm eq} = e^{-\beta\epsilon_i}/Z$,

$$F(T) = \tau\beta^4 \sum_i p_i^{\rm eq} \sum_{j\neq i} \frac{|\partial_\beta \Gamma_{ij}|^2}{\Gamma_{ij}}. \tag{2}$$

Our main goal will be to maximize (2) by choosing an optimal energy structure of the probe, which determines the functional behavior of the rates Γ_{ij}. A key figure of merit will be its scaling with respect to the number of levels, which is an important cost in terms of the dimensionality of the system. For example, a probe consisting of n two-level spin states is related to the number of levels as $N = 2^n$. One should bear in mind that the optimal scaling of $F(T)$ will at most be linear in N due to the bound

$$F(T) \leqslant \tau\beta^4 (N-1) \max_{\{i,j\}} \frac{|\partial_\theta \Gamma_{ij}|^2}{\Gamma_{ij}}. \tag{3}$$

While this bound is not necessarily tight in a continuously monitored setup, one can saturate it by using a measure-and-reset strategy following a result from Ref. [48]. That is, if we were allowed to reset the system after each jump, we would choose an effective two-level Hamiltonian structure, with a ground state and an $(N-1)$-fold degenerate excited state at a gap ϵ_j chosen such that the fraction $\frac{|\partial_\theta \Gamma_{0j}|^2}{\Gamma_{0j}}$ is maximized independent of N. After each measurement, one would reset the system to the ground state, which comes with an unwanted resource cost. Fortunately we now demonstrate that the linear scaling suggested by (3) is in fact achievable in the continuous approach, avoiding this need to reset.

Fermionic sample. We first look at the estimation of a fermionic sample with a spectral density taken in the wide-band limit. The transition rates of the probe are proportional to the Fermi occupation $n_F(\omega_{ji})$ of each excitation

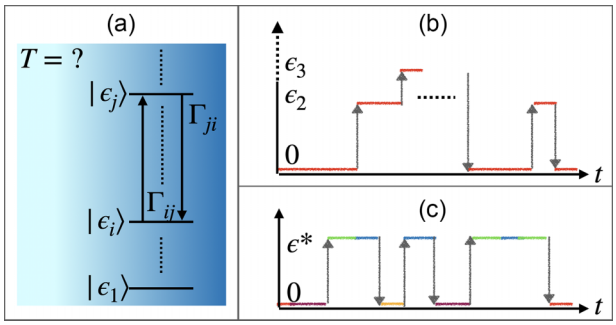

FIG. 1. (a) An N-level probe is in contact with a thermal bath at temperature T. The transition rates between different energy levels, Γ_{ij}, are temperature dependent. (b) The trajectory that the N-level system takes contains information about the temperature. The precision with which the trajectory can estimate the temperature highly depends on the energy structure. (c) The optimal energy structure—as we find in this Letter—is effectively two-level, with ground state and excited state degeneracy that both increase linearly with N, and at some optimal gap ϵ^*. In the figure we have color coded the degenerate gaps to tell them apart visually.

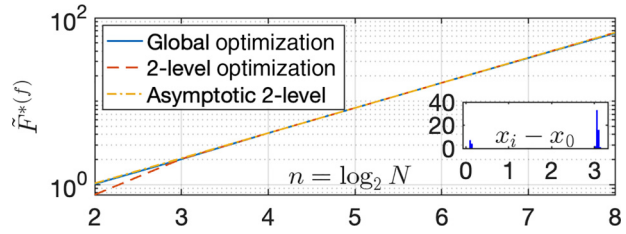

FIG. 2. Numerical results for the optimal dimensionless FI rate (6). We compare the exact solution obtained via global optimization with the optimal two-level ansatz (7) (optimized over N_0 and x). The analytic value (8) obtained in the asymptotic $N \gg 1$ limit is also plotted and shows good agreement with the exact solution for $n \geqslant 3$. Inset: This plot depicts a histogram of the energy levels found from a global optimization for $n = 6$. Our numerics suggest that an effective two-level structure is optimal. We have thus also considered an effective two-level ansatz which can be optimized more efficiently due to fewer parameters. The FI rate of the two-level ansatz is shown by the red curve in the primary figure which also as one can see agrees very well with the global optimum for $n \geqslant 3$.

$\omega_{ji} \equiv \epsilon_j - \epsilon_i$, namely

$$\Gamma_{ij} = \gamma n_F(\omega_{ji}) = \gamma[e^{\beta\omega_{ji}} + 1]^{-1}, \tag{4}$$

with γ the coupling strength. It follows from (2) that the FI is

$$F(T) = \gamma\tau\beta^4 \sum_i p_i^{\mathrm{eq}} \sum_{j\neq i} \omega_{ji}^2 \frac{e^{2\beta\omega_{ji}}}{[1+e^{\beta\omega_{ji}}]^3} = \gamma\tau\beta^2\tilde{F}^{(f)}, \tag{5}$$

where we have identified the dimensionless FI rate,

$$\tilde{F}^{(f)} := \sum_i p_i^{\mathrm{eq}} \sum_{j\neq i} x_{ji}^2 \frac{e^{2x_{ji}}}{[1+e^{x_{ji}}]^3}, \tag{6}$$

and set $x_{ij} = \beta\omega_{ij}$. The goal is now to optimize $\tilde{F}^{(f)}$ over the set of $\{x_i = \beta\epsilon_i\}_{i=0}^{N-1}$. As a nonlinear problem, we first turn to numerics and run an optimization in MATLAB [64]. For $N = 2^n$ with $n \in \{2, \ldots, 8\}$ we observe two situations: (1) The optimal value $\tilde{F}^{*(f)} = \max_{\{x_i\}} \tilde{F}^{(f)}$ grows linearly with N. (2) For $n \geqslant 3$, an effective two-level degenerate structure is able to reach the global optimum with small numerical error—see Fig. 2. We therefore adopt an ansatz consisting of N_0 ground state levels and $N - N_0$ excited state levels, with a single dimensionless gap $x = \beta\omega$. In this case the FI rate reads

$$\tilde{F}_{\mathrm{2lev}}^{(f)} = \frac{N_0(N-N_0)}{N_0 + (N-N_0)e^{-x}} \left(\frac{x^2 e^{2x}}{[1+e^x]^3} + \frac{x^2 e^{-3x}}{[1+e^{-x}]^3} \right). \tag{7}$$

To optimize further, there are two remaining free parameters N_0 and x. Figure 3 shows that x is tending to a constant for large n, while the degeneracy appears to exponentially increase with n. To see this analytically we look at the $N \gg 1$ regime and treat N_0 as a continuous number, so that it can be expressed as a fraction $N_0 = CN$. Straightforwardly one can show that, for a fixed x, the optimal solution of C depends on the gap and reads $C(x) = 1/(1 + e^{x/2})$. Substituting back in the FI rate, we get

$$\begin{aligned} \tilde{F}_{\mathrm{2lev}}^{(f)} &= Nx^2 \frac{C(x)[1-C(x)]}{C(x) + [1-C(x)]e^{-x}} \left(\frac{e^{2x}}{(e^x+1)^3} + \frac{e^{-3x}}{(e^{-x}+1)^3} \right) \\ &= Nf(x). \end{aligned} \tag{8}$$

Interestingly, the function $f(x)$ has a unique maximum which can be found numerically. Therefore, for large enough N, we have the optimal structure and its corresponding Fisher information rate as $\tilde{F}_{\mathrm{2lev}}^{*(f)} \approx 0.2596N$, $x^* \approx 2.9682$, and $N_0^* \approx \max\{\mathrm{floor}(0.1848N), 1\}$. As a comparison, note that the bound in Eq. (3) that requires resetting the probe after each measurement, gives $x_{\mathrm{reset}}^* \approx 2.5331$, and $F_{\mathrm{reset}}^{*(f)} \approx 0.4052N$. Finally, a key observation is that the width of the Fisher information for the optimal continuously monitored thermometer does not shrink with $n = \log_2 N$; it actually remains constant, as can be seen from its expression above and also Fig. 3, thus avoiding the fate of the optimal equilibrium thermometer [19] when our initial knowledge of the temperature is limited—that is, global thermometry. While using adaptive schemes as proposed in Ref. [29] may improve the precision up to a coefficient, the scaling is not compromised if one does not use them. In the Supplemental Material [65], we furthermore show that even if the degenerate energy levels are not perfectly prepared, the linear scaling survives, adding an additional layer of robustness and practicality into the optimal scaling.

Bosonic sample. We now investigate the performance of the probe when coupled to a bosonic sample. In this case the transition rates are given by $\Gamma_{ij} = \kappa(|\omega_{ji}|)|n_B(\omega_{ji})|$ where $n_B(\omega) = [e^{\beta\omega} - 1]^{-1}$ is the Bose-Einstein distribution and $\kappa(\omega)$ represents the spectral density. Here, we restrict

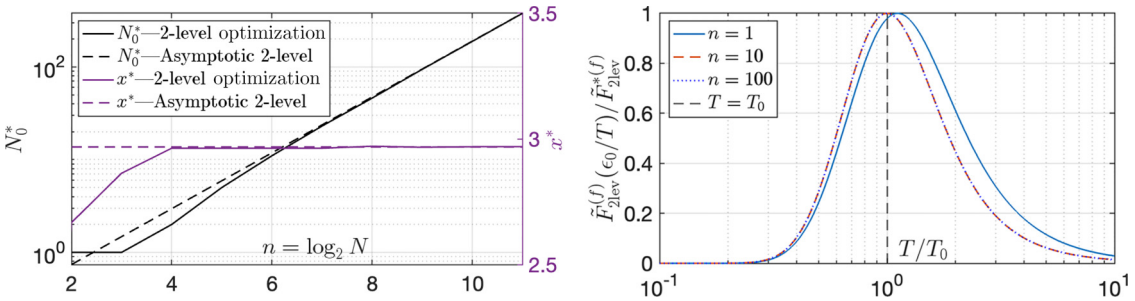

FIG. 3. Left: Plot of the optimal free parameters for the two-level ansatz (7) for a fermionic probe as a function of $n = \log_2 N$, with optimal ground state degeneracy N_0^* (black) and optimal gap x^* (red). The dashed lines give the values for the asymptotic optimal solution (8). Right: Plot of FI rate normalized by its maximum value, for different values of n. Here, the gap is tuned to $\epsilon_0 = x^* T_0$, such that the thermometer is optimal for some assumed temperature T_0.

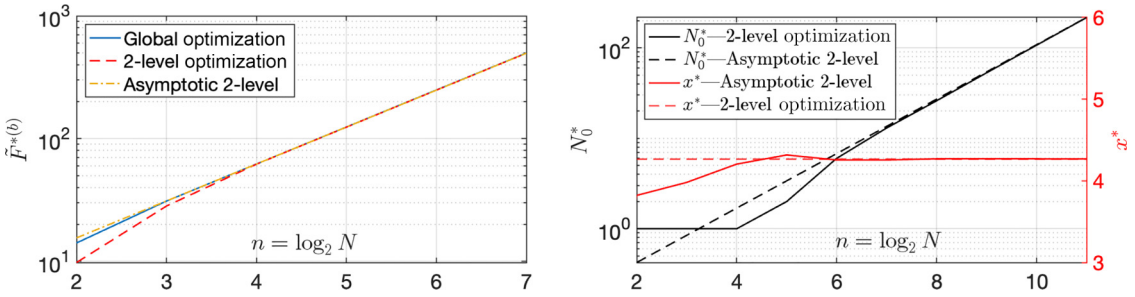

FIG. 4. Left: The optimal FI rate (9) for a bosonic case with ohmicity $s = 2$, using a global optimization (solid) and the two-level ansatz (10) (red dashed). The asymptotic values are taken from Table I. Right: The optimal energy gap x^* (red) for the two-level ansatz and its asymptotic prediction from Table I and the ground state degeneracy of the optimal structure for the two-level ansatz (black) and its asymptotic behavior from Table I.

attention to super Ohmic spectral densities of the form $\kappa(\omega) = \gamma\omega^s$ with $s > 1$.

In analogy with (6), the figure of merit for the probe performance is the FI rate,

$$\tilde{F}^{(b)} := \frac{F(T)}{\gamma\tau T^{2+s}} = \sum_i p_i^{\mathrm{eq}} \sum_{j\neq i} \frac{x_{ji}^{2+s} e^{2x_{ji}}}{|e^{x_{ji}} - 1|^3}, \tag{9}$$

where we combined (2) with the bosonic decay rates. Note that in this case, the nonflat spectral density means that we must divide by an additional factor T^s to preserve scale invariance [66].

Similar to the fermionic case, numerics suggest again that—for $n > 3$—a 2-level energy structure globally optimizes (9). Taking a 2-level ansatz for (9) gives

$$\tilde{F}_{\mathrm{2lev}}^{(b)} = \frac{N_0(N - N_0)}{N_0 + (N - N_0)e^{-x}} \left(\frac{x^{2+s}e^{2x}}{|e^x - 1|^3} + \frac{x^{2+s}e^{-3x}}{|e^{-x} - 1|^3} \right), \tag{10}$$

We numerically optimize this two-level structure to find the optimal N_0 and x as depicted in Fig. 4, and see similar qualitative behavior as in the fermionic case. Looking at the asymptotic regime $N \gg 1$ as we did with (8), the FI rate is

$$\begin{aligned} \tilde{F}_{\mathrm{2lev}}^{(b)} &= N \frac{C(x)[1 - C(x)]}{C(x) + [1 - C(x)]e^{-x}} \left(\frac{x^{2+s}e^{2x}}{|e^x - 1|^3} + \frac{x^{2+s}e^{-3x}}{|e^{-x} - 1|^3} \right) \\ &= Nb(x). \end{aligned} \tag{11}$$

The ohmicity parameter is determinant on the optimal gap, the ground state degeneracy, and the corresponding FI. These are summarized in Table I for various ohmicity parameters. Again, if we compare with the reset-and-measure setting bound in Eq. (3), we would get $F_{\mathrm{reset}}^{*(b)} = \{1.6786, 2.7144, 4.9953, 21.5120\}N$ and $x_{\mathrm{reset}}^* = \{2.7144, 3.0430, 3.7240, 4.8890\}$, respectively, for $s = \{1^+, 1.5, 2, 3\}$.

TABLE I. The optimal values of the gap and the corresponding ground state degeneracy fraction C^* and the FI coefficient $b(x^*)$ defined in (11) for various choices of spectral density (SD). The case with $s = 1^+$ is calculated for $s = 1 + \epsilon$ and then taken at the limit of $\epsilon \to 0$.

SD	x^*	C^*	$b(x^*)$
$s = 1^+$	3.0880	0.1760	1.0508
$s = 1.5$	3.7195	0.1347	1.9403
$s = 2$	4.2681	0.1058	3.8782
$s = 3$	5.2706	0.0669	18.4880

Discussion. We have demonstrated that the optimal energy structure of a continuously monitored thermometer, for both fermionic and bosonic samples, is an effective two-level system that can achieve linear scaling with respect to the number of levels. To complete the picture, we also derive the corresponding maximum-likelihood estimator for this setup in Appendix A of the Supplemental Material which allows saturation of the Cramer-Rao bound used implicitly throughout our analysis [65]. There are two distinct factors that highlight the significant advantages offered by the continuous monitoring approach. First, there is a clear exponential improvement over the equilibrium thermometer; in the latter case the FI is known to scale with $\log^2 N$, as we recap in Appendix B of the Supplemental Material [65]. Second, we have found that the width of the FI remains constant with increasing probe size. This means that it is possible to achieve a linear scaling without requiring an adaptive feedback approach. We further show in Appendix C of the Supplemental Material [65] that the optimal probe performs similarly even when one only has access to the average populations, as quantified in terms of the empirical FI rate [59]. On top of that, we also show in Appendix D of the Supplemental Material [65] that the linear scaling remains intact even in the presence of imperfections in preparation of an optimal two-level structure. These add another layer of robustness to the results. In summary, taking into account the various resources needed for optimal thermometry, our findings suggest that the continuous monitoring approach performs best.

It should be emphasized that these results are predicated on the assumption of the Markovian rate equation (1). An interesting future direction would be to explore the role of non-Markovian effects on the performance of the optimal monitored thermometer. We have also neglected to study the thermometry of sub-Ohmic samples since such systems are not well described by (1). A promising subject for future studies is thus to consider non-Markovian dynamics beyond the rate equation.

Acknowledgments. The authors acknowledge TU Wien Bibliothek for financial support through its Open Access Funding Programme. This research was funded in part by

the Austrian Science Fund (FWF) (10.55776/I6047). This research was supported by the European Research Council (Consolidator grant 'Cocoquest' 101043705). H.J.D.M. acknowledges funding from a Royal Society Research Fellowship (URF/R1/231394). This project is co-funded by the European Union (Quantum Flagship project ASPECTS, Grant Agreement No. 101080167).

Views and opinions expressed are however those of the authors only and do not necessarily reflect those of the European Union, REA, or UKRI.

[1] L. Levitin, H. van der Vliet, S. Dimitriadis, T. Theisen, M. Lucas, A. D. Córcoles, J. Nyeki, A. Casey, G. Creeth, I. Farrer, D. Ritchie, J. Nicholls, and J. Saunders, Nat. Commun. **13**, 667 (2022).

[2] M. Sarsby, N. Yurttagül, and A. Geresdi, Nat. Commun. **11**, 1492 (2020).

[3] I. Bloch, Nat. Phys. **1**, 23 (2005).

[4] X. Chen and B. Fan, Rep. Prog. Phys. **83**, 076401 (2020).

[5] C. Nayak, S. H. Simon, A. Stern, M. Freedman, and S. Das Sarma, Rev. Mod. Phys. **80**, 1083 (2008).

[6] M. Z. Hasan and C. L. Kane, Rev. Mod. Phys. **82**, 3045 (2010).

[7] T. Langen, R. Geiger, and J. Schmiedmayer, Annu. Rev. Condens. Matter Phys. **6**, 201 (2015).

[8] T. Langen, R. Geiger, M. Kuhnert, B. Rauer, and J. Schmiedmayer, Nat. Phys. **9**, 640 (2013).

[9] N. M. Myers, O. Abah, and S. Deffner, AIP Adv. **4**, 027101 (2022).

[10] G. Mihailescu, S. Campbell, and A. K. Mitchell, Phys. Rev. A **107**, 042614 (2023).

[11] T. P. Purdy, P.-L. Yu, N. S. Kampel, R. W. Peterson, K. Cicak, R. W. Simmonds, and C. A. Regal, Phys. Rev. A **92**, 031802(R) (2015).

[12] M. Mehboudi, A. Lampo, C. Charalambous, L. A. Correa, M. A. García-March, and M. Lewenstein, Phys. Rev. Lett. **122**, 030403 (2019).

[13] L. Oghittu and A. Negretti, Phys. Rev. Res. **4**, 023069 (2022).

[14] M. M. Khan, M. Mehboudi, H. Terças, M. Lewenstein, and M. A. Garcia-March, Phys. Rev. Res. **4**, 023191 (2022).

[15] G. Planella, M. F. B. Cenni, A. Acín, and M. Mehboudi, Phys. Rev. Lett. **128**, 040502 (2022).

[16] M. T. Mitchison, T. Fogarty, G. Guarnieri, S. Campbell, T. Busch, and J. Goold, Phys. Rev. Lett. **125**, 080402 (2020).

[17] A. K. Srivastava, U. Bhattacharya, M. Lewenstein, and M. Płodzień, arXiv:2311.14524.

[18] M. Mehboudi, A. Sanpera, and L. A. Correa, J. Phys. A: Math. Theor. **52**, 303001 (2019).

[19] L. A. Correa, M. Mehboudi, G. Adesso, and A. Sanpera, Phys. Rev. Lett. **114**, 220405 (2015).

[20] G. De Palma, A. De Pasquale, and V. Giovannetti, Phys. Rev. A **95**, 052115 (2017).

[21] A. De Pasquale and T. M. Stace, in *Thermodynamics in the Quantum Regime*, edited by F. Binder, L. Correa, C. Gogolin, J. Anders, and G. Adesso, Fundamental Theories of Physics Vol. 195 (Springer, Cham, 2018), pp. 503–527.

[22] K. V. Hovhannisyan and L. A. Correa, Phys. Rev. B **98**, 045101 (2018).

[23] J. Glatthard, K. V. Hovhannisyan, M. Perarnau-Llobet, L. A. Correa, and H. J. D. Miller, Quantum **7**, 1190 (2023).

[24] P. P. Potts, J. B. Brask, and N. Brunner, Quantum **3**, 161 (2019).

[25] M. R. Jorgensen, P. P. Potts, M. G. A. Paris, and J. B. Brask, Phys. Rev. Res. **2**, 033394 (2020).

[26] J. Rubio, J. Anders, and L. A. Correa, Phys. Rev. Lett. **127**, 190402 (2021).

[27] J. Glatthard, J. Rubio, R. Sawant, T. Hewitt, G. Barontini, and L. A. Correa, PRX Quantum **3**, 040330 (2022).

[28] G. O. Alves and G. T. Landi, Phys. Rev. A **105**, 012212 (2022).

[29] M. Mehboudi, M. R. Jorgensen, S. Seah, J. B. Brask, J. Kolodynski, and M. Perarnau-Llobet, Phys. Rev. Lett. **128**, 130502 (2022).

[30] J. Boeyens, S. Seah, and S. Nimmrichter, Phys. Rev. A **104**, 052214 (2021).

[31] T. M. Stace, Phys. Rev. A **82**, 011611(R) (2010).

[32] W.-K. Mok, K. Bharti, L.-C. Kwek, and A. Bayat, Commun. Phys. **4**, 62 (2021).

[33] G. W. Walker, V. C. Sundar, C. M. Rudzinski, A. W. Wun, M. G. Bawendi, and D. G. Nocera, Appl. Phys. Lett. **83**, 3555 (2003).

[34] L. D. Carlos and F. Palacio, *Thermometry at the Nanoscale: Techniques and Selected Applications*, edited by L. Dias Carlos and F. Palacio (Royal Society of Chemistry, London, 2015).

[35] M. Płodzień, R. Demkowicz-Dobrzański, and T. Sowiński, Phys. Rev. A **97**, 063619 (2018).

[36] C. T. Nguyen, R. E. Evans, A. Sipahigil, M. K. Bhaskar, D. D. Sukachev, V. N. Agafonov, V. A. Davydov, L. F. Kulikova, F. Jelezko, and M. D. Lukin, Appl. Phys. Lett. **112**, 203102 (2018).

[37] L.-S. Guo, B.-M. Xu, J. Zou, and B. Shao, Phys. Rev. A **92**, 052112 (2015).

[38] G. Salvatori, A. Mandarino, and M. G. A. Paris, Phys. Rev. A **90**, 022111 (2014).

[39] M. Mehboudi, M. Moreno-Cardoner, G. D. Chiara, and A. Sanpera, New J. Phys. **17**, 055020 (2015).

[40] M. Salado-Mejía, R. Román-Ancheyta, F. Soto-Eguibar, and H. M. Moya-Cessa, Quantum Sci. Technol. **6**, 025010 (2021).

[41] P. Abiuso, P. A. Erdman, M. Ronen, F. Noe, G. Haack, and M. Perarnau-Llobet, Quantum Sci. Technol. **9** 035008 (2024).

[42] F. Ivander, N. Anto-Sztrikacs, and D. Segal, Phys. Rev. E **108**, 014130 (2023).

[43] S. Dooley, W. J. Munro, and K. Nemoto, Phys. Rev. A **94**, 052320 (2016).

[44] A. J. Hayes, S. Dooley, W. J. Munro, K. Nemoto, and J. Dunningham, Quantum Sci. Technol. **3**, 035007 (2018).

[45] N. Anto-Sztrikacs, H. J. D. Miller, A. Nazir, and D. Segal, Phys. Rev. A **109**, L060201 (2024).

[46] M. Brunelli, S. Olivares, and M. G. A. Paris, Phys. Rev. A **84**, 032105 (2011).

[47] V. Cavina, L. Mancino, A. De Pasquale, I. Gianani, M. Sbroscia, R. I. Booth, E. Roccia, R. Raimondi, V. Giovannetti, and M. Barbieri, Phys. Rev. A **98**, 050101(R) (2018).

[48] P. Sekatski and M. Perarnau-Llobet, Quantum **6**, 869 (2022).

[49] F. S. Luiz, A. de O. Junior, F. F. Fanchini, and G. T. Landi, Phys. Rev. A **105**, 022413 (2022).
[50] R. R. Rodríguez, M. Mehboudi, M. Horodecki, and M. Perarnau-Llobet, New J. Phys. **26**, 013046 (2024).
[51] T. M. Mendonça, D. O. Soares-Pinto, and M. Paternostro, arXiv:2407.21618.
[52] S. Brattegard and M. T. Mitchison, Phys. Rev. A **109**, 023309 (2024).
[53] S. Seah, S. Nimmrichter, D. Grimmer, J. P. Santos, V. Scarani, and G. T. Landi, Phys. Rev. Lett. **123**, 180602 (2019).
[54] S. Gammelmark and K. Molmer, Phys. Rev. Lett. **112**, 170401 (2014).
[55] A. H. Kiilerich and K. Molmer, Phys. Rev. A **89**, 052110 (2014).
[56] M. A. C. Rossi, F. Albarelli, D. Tamascelli, and M. G. Genoni, Phys. Rev. Lett. **125**, 200505 (2020).
[57] F. Albarelli and M. G. Genoni, Phys. Lett. A **494**, 129260 (2024).
[58] J. Boeyens, B. Annby-Andersson, P. Bakhshinezhad, G. Haack, M. Perarnau-Llobet, S. Nimmrichter, P. P. Potts, and M. Mehboudi, New J. Phys. **25**, 123009 (2023).
[59] J. A. Smiga, M. Radaelli, F. C. Binder, and G. T. Landi, Phys. Rev. Res. **5**, 033150 (2023).
[60] J. Zhang, Y.-x. Liu, R.-B. Wu, K. Jacobs, and F. Nori, Phys. Rep. **679**, 1 (2017).
[61] R. Vijay, C. Macklin, D. H. Slichter, S. J. Weber, K. W. Murch, R. Naik, A. N. Korotkov, and I. Siddiqi, Nature (London) **490**, 77 (2012).
[62] J. Kong, R. Jiménez-Martínez, C. Troullinou, V. G. Lucivero, G. Tóth, and M. W. Mitchell, Nat. Commun. **11**, 2415 (2020).
[63] G. T. Landi, M. J. Kewming, M. T. Mitchison, and P. P. Potts, PRX Quantum **5**, 020201 (2024).
[64] All MATLAB codes are publicly available on this GitHub repository, https://github.com/Mehboudi/Thermometry-with-Continious-Monitoring-using-N-level-probes.git.
[65] See Supplemental Material at http://link.aps.org/supplemental/10.1103/PhysRevA.111.L020401 for a derivation of the maximum-likelihood estimator; comparison to equilibrium thermometry; the empirical Fisher information; and robustness to energy structure, which includes Ref. [67].
[66] J. Rubio, Quantum Sci. Technol. **8**, 015009 (2023).
[67] D. E. Knuth, SIGACT News **8**, 18 (1976).